Materials Science and Engineering A 527 (2010) 3929–3935

Contents lists available at ScienceDirect

Materials Science and Engineering A

journal homepage: www.elsevier.com/locate/msea

Influence of processing parameters on mechanical properties of Ti–6Al–4V alloy fabricated by MIM

G.C. Obasi*, O.M. Ferri, T. Ebel, R. Bormann

GKSS Research Centre, Institute of Materials Research, Max-Planck-Straße 1, D-21502 Geesthacht, Germany

ARTICLE INFO

Article history:
Received 14 August 2009
Received in revised form 24 February 2010
Accepted 25 February 2010

Keywords:
Metal injection molding
Debinding parameters
Sintering parameters
Mechanical properties

ABSTRACT

This study presents the results of systematic variation of essential processing parameters with regard to thermal debinding and sintering of components fabricated by MIM using Ti–6Al–4V powder. The investigation aims at the understanding of the particular influence these parameters have on the mechanical properties of the sintered parts. This study shows that the debinding parameters appear to be rather uncritical, whereas sintering and cooling rates as well as maximum temperature are important in terms of their effect on tensile strength. Contrary to the strength, the ductility remains nearly unaffected. Based on these results, samples displaying yield strength of 757 MPa, UTS of 861 MPa and a plastic elongation of more than 14% were produced. These values meet the requirements of the ASTM B348-02 for titanium alloy grade 23.

1. Introduction

The excellent properties of Ti–6Al–4V alloy such as high specific strength, high corrosion resistance in many media, and excellent biocompatibility have attracted attention for the last decades and make this alloy an excellent choice for many applications, including medical implants, automotive components, and air craft parts [1]. However, the utilisation of this alloy has been limited due to the high costs related to the raw material, the multi-step fabrication process, and associated geometry design constraints. Metal Injection Molding (MIM) is a manufacturing process candidate that can be applied in order to overcome some of these drawbacks.

MIM offers a net-shape or near net-shape fabrication route for making complex shaped parts in large volumes. In the past few years, the development of this process has been successful. The problem of contamination with oxygen, nitrogen and carbon during debinding and sintering operations, which strongly influences the mechanical properties, can largely be overcome. Parts based on Ti–6Al–4V with reasonable strength-levels and large plastic elongations can be achieved today (e.g. [2–4]). However, with respect to further optimization, the effect of microstructural features such as final porosity, size of the lamellar colonies, and interstitial element content on the mechanical properties of Ti–6Al–4V alloy components fabricated by MIM is not totally understood.

In this study, the MIM process was used to produce samples using Ti–6Al–4V alloy powder <45 μm with d_{90} = 41 μm. Sintering and debinding conditions were varied in order to analyse the effect on the mechanical and microstructural properties of the components.

2. Sample preparation

The samples were prepared by a Metal Injection Molding process as described in [5] using a wax and polymer based feedstock. Ti–6Al–4V ELI (ASTM grade 23) gas atomised powder of spherical shape with a particle diameter d_{90} of 41 μm was used in this study. The chemical composition of the powder according to the supplier is given in Table 1.

The binder system used was a mixture of 35 wt.% polyethylene, 5 wt.% stearic acid and 60 wt.% paraffin wax. The feedstock used in the experiments had a binder system fraction of 8.5 wt. % (31 vol.%), except during the investigation of the influence of sintering time, where a feedstock with 10 wt.% (35 vol.%) binder was used. The metal powder and the binder system were mixed in a Z-blade mixer under argon atmosphere. After granulation, the feedstock was injection molded into a standard "dog bone" shape tensile specimens, with a nominal length of about 89 mm and thickness of 5 mm.

Afterwards the paraffin wax in the tensile specimens (green part) was removed by chemical debinding with heptane at 313 K for 20 h. The thermal debinding and the sintering of five samples of the tensile specimens for each condition were performed in a cold-wall furnace with tungsten heating elements and molybdenum

* Corresponding author at: The University of Manchester, UK Materials Science Centre, Grosvenor Street, Manchester M1 7HS, United Kingdom.
E-mail address: Gideon.obasi@postgrad.manchester.ac.uk (G.C. Obasi).

0921-5093/$ – see front matter © 2010 Elsevier B.V. All rights reserved.
doi:10.1016/j.msea.2010.02.070

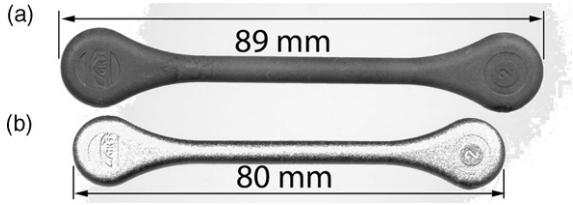

Fig. 1. Standard tensile specimen "dog bone" (a) green part and (b) as sintered part.

shield packs. The size of the process chamber was around 10 l. The thermal debinding process was conducted under argon atmosphere followed by sintering under high vacuum ($\sim 10^{-4}$ mbar). The five samples were placed near to each other at centre of the process chamber. Prior to sintering the furnace was calibrated and no significant temperature gradient in the region where the samples were sintered was observed. The sintered compacts had a nominal length between 79 and 80 mm and a typically thickness around 4.3 mm. Fig. 1 shows the specimens in green and sintered stages.

After sintering, the levels of oxygen, carbon and nitrogen were determined using a conventional LECO melt extraction system. The apparent density of the five sintered parts was measured by the immersion method outlined in ASTM B311.

The tensile tests were carried out on three samples (as sintered) using a servo-hydraulic structural test machine equipped with a 100 kN load cell at room temperature. A strain rate of $3.5 \times 10^{-5}\ s^{-1}$ was applied.

Optical microscopy (Olympus PMG3) and scanning electron microscopy (ZEISS-DSM962) were used in order to investigate the sintered microstructure and the tensile fracture surface of the three samples, respectively. An imaging analysis system, Olympus Soft Image Solution analysis pro software, was applied in order to estimate the pore size. For these analyses, at least 500 pores were measured for each different configuration. The pore shape was determined by the form factor:

$$\text{Form Factor} = \frac{4\pi A}{P^2} \quad (1)$$

where A = area of pore, and P = circumference of pore in plane of analysis.

A form factor of 1 represents a circular pore in the plane of analysis and as the number decreases from 1, the degree of irregularity increases. In addition, a linear intercept technique (ASTM E112-96) was applied on five optical and SEM images of each of the three tensile samples for the estimation of the average α colony size and the α lamellae width, respectively.

3. Results and discussion

The heating rate to debinding temperature dT_{debind}, the heating rate to sintering temperature dT_{sinter}, the sintering temperature, the sintering time, and the cooling rate were identified as essential parameters, which could influence the mechanical properties of the sintered part. All parameters could potentially change the content of interstitials, the final density, grain size or grain structure. In the following sections, the results from the variation of these parameters with respect to mechanical and microstructural properties are reported.

All sintered samples described in the following sections were analysed with respect to their content of interstitial elements O, N and C, because of the influence of these interstitial impurities on strength and ductility. However, the deviation in these contents during variation of the debinding and sintering parameters was not significant. The analysed average values of all samples were 2154 ± 91 μg/g oxygen, 378 ± 26 μg/g carbon and 182 ± 31 μg/g nitrogen.

Table 1
Chemical composition of the powder (wt.%).

Element	Al	V	C	Fe	O	N	H	Ti
wt.%	6.14	4.0	0.020	0.150	0.100	0.010	0.004	Bal.

Table 2
Variation of sintering temperature.

Temperature (K)	Tensile properties			Microstructural features	
	Yield stress (MPa)	UTS (MPa)	Elongation (%)	Average colony size (μm)	Densification (%)
1523	703 ± 6	806 ± 3	13.7 ± 1	92 ± 3	96.2
1573	720 ± 4	821 ± 2	14.0 ± 2	93 ± 2	96.4
1623	728 ± 5	832 ± 2	13.4 ± 1	102 ± 2	97.1
1673	744 ± 6	846 ± 5	14.8 ± 2	120 ± 3	97.3

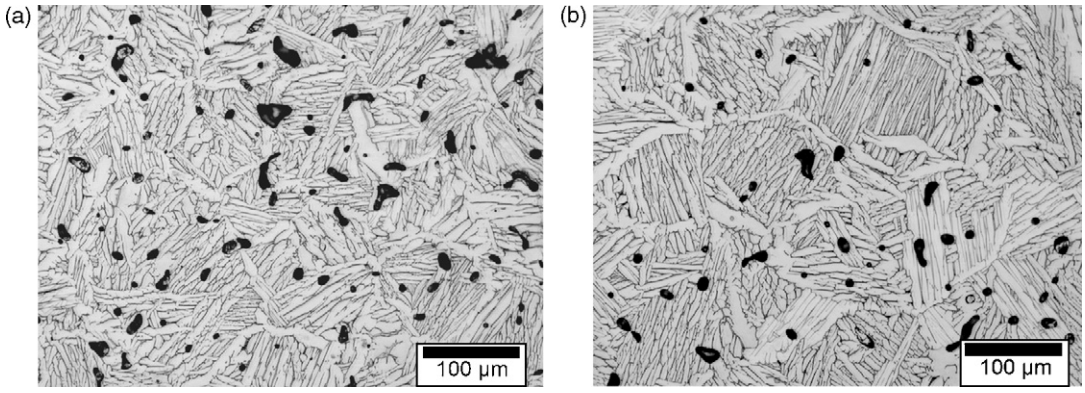

Fig. 2. Optical micrographs of samples sintered at different temperatures (a) at 1523 K (b) at 1673 K, revealing different colony size.

Table 3
Mean pore size, standard deviation and P_{90} (90% of the pores analyzed were below this value) for MIM samples sintered at different temperatures.

Temperature (K)	Mean pore size (μm)	Standard deviation (μm)	P_{90} (μm)
1523	11	7	17
1573	12	7	19
1623	12	6	17
1673	13	7	19

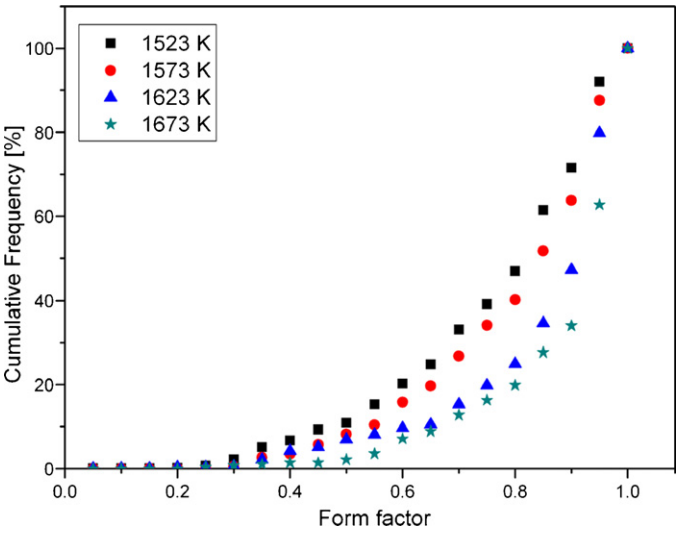

Fig. 3. Influence of the maximum sintering temperature on the pore shape.

Therefore, no dependence of these values on the varied processing parameters could be detected. Thus, the pick up of interstitials during processing was considered to be constant within this investigation and was not taken into account in the following discussion.

3.1. Variation of sintering temperature

Table 2 shows the influence of maximum sintering temperature on the tensile properties and the microstructure of the sintered samples. The yield strength and the UTS increase significantly as sintering temperature increases; however, no clear effect of the maximum sintering temperature on the plastic elongation was observed.

Fig. 2(a and b) shows the optical micrographs of two samples sintered at 1523 K and 1673 K. They reveal a typical fully lamellar microstructure with the additional presence of pores.

As illustrated in Table 3 no significant influence of maximum sintering temperature on the pore size was observed.

On the other hand, the pore shape is clearly affected by the maximum sintering temperature. With increasing the maximum sintering temperature the pore shape becomes more circular as demonstrated in Fig. 3.

As expected, the observed higher strength for samples sintered at higher temperature can be related to differences in the microstructural features. The level of densification (amount of pores) seems to be the most relevant parameter that influenced the tensile strength. This result is in line with previous works [2–4] where samples with lower porosity exhibited higher yield strength and UTS.

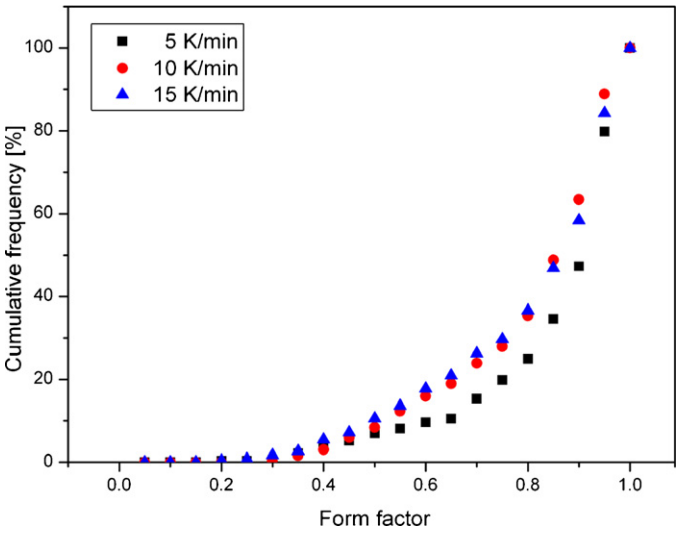

Fig. 4. Influence of the sintering heating rate on the pore shape.

Diametrical to the positive effect of the lower porosity on strength should be the coarsening of the α colony size observed for samples sintered at higher temperatures (Table 2). This significant coarsening effect was already investigated by Itoh et al. [3] and Zhang et al. [4], and this effect is related to the predominant influence of the coarsening mechanism over densification during sintering at high temperatures. However, with respect to tensile strength, the positive effect of the higher density overcomes the negative effect of the coarser grains. On the other hand, fine microstructures are typically desired for components that will be exposed to e.g. cycle loading. Therefore, in order to compromise densification and grain size, the maximum sintering temperature used for the following experiments was 1623 K.

3.2. Variation of heating rate to sintering temperature dT_{sinter}

The heating rate dT_{sinter} describes the temperature change per minute during heating from debinding to maximum sintering temperature. Table 4 shows the measured properties of samples sintered at the same maximum sintering temperature (1623 K), but with different heating rates.

As indicated in Table 4, applying a heating rate dT_{sinter} of 15 K/min promotes a certain deterioration of the tensile properties. This is especially true in terms of plastic elongation. Such behaviour is not fully understood yet, but it is possible to assume that at a heating rate of 15 K/min, the coarsening process overcomes the densification process faster than it does at slower heating rate. This assumption is in agreement with the final densification results presented in Table 4. Additionally, the size of the pores apparently increased due to faster heating rate (Table 5).

Table 4
Variation of sintering heating rate. Sintering temperature 1623 K.

Heating rate dT_{sinter} (K/min)	Tensile properties			Microstructural features	
	Yield stress (MPa)	UTS (MPa)	Elongation (%)	Average colony size (μm)	Densification (%)
5	728 ± 5	832 ± 2	13.4 ± 0.5	102 ± 3	97.1
10	731 ± 3	832 ± 3	14.9 ± 1.7	104 ± 2	96.8
15	723 ± 5	825 ± 3	11.2 ± 0.4	112 ± 5	96.6

Table 5
Mean pore size, standard deviation and P_{90}, for MIM samples sintered at1623 K, with different sintering heating rate.

Heating rate dT_{sinter} (K/min)	Mean pore size (μm)	Standard deviation (μm)	P_{90} (μm)
5	12	6	17
10	12	8	20
15	16	10	27

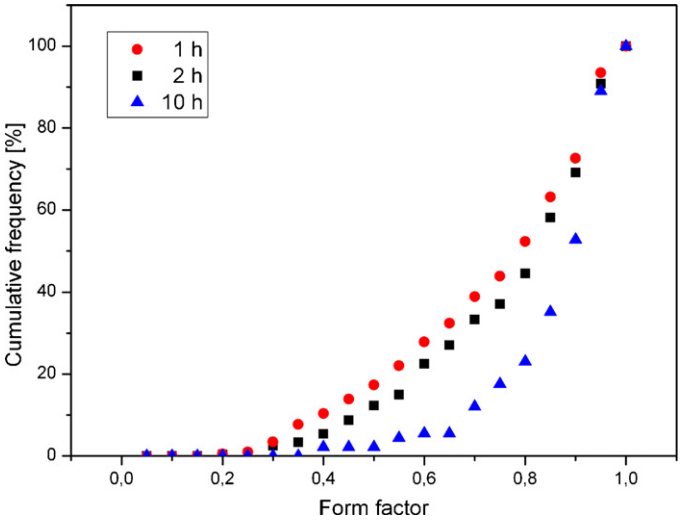

Fig. 5. Influence of the sintering time on the pore shape.

Another parameter that was influenced by the heating rate was the shape of the pores. As illustrated in Fig. 4, faster heating rate promoted more irregular pore morphology.

Consequently, the deterioration of the tensile elongation for the samples sintered with a heating rate of 15 K/min could be related to a combination of effects such as: relative larger grain size, relative higher level of porosity together with the tendency of the existence of larger and more irregular pores. This is an indication of a maximum rate existing above 10 K/min which should not be exceeded to avoid embrittlement.

3.3. Variation of sintering time

The effect of changing the sintering time at the isotherm of 1623 K was investigated on samples with a binder content of 35 vol.% (referring to 10 wt.%). The comparison with samples with 31 vol.% binder content exposed to the same process revealed a lower density of the 35 vol.% samples, probably due to a slightly larger distance between the particles prior to sintering.

As expected, sintering for only 1 h instead of 2 h reduced the strength as seen in Table 6. Again, the reason for this is assumed to be the lower densification.

As illustrated in Table 7 the samples sintered with different sintering time exhibited approximately the same pore size. On the other hand, as time increases the pores tend to be more regular (Fig. 5). Although significant difference in the amount and shape of the pores were observed between samples sintered during 1 and 10 h, no systematic relationship existed between porosity and plastic elongation.

Applying a prolonged sintering time of 10 h increased densification and strength significantly. No additional oxygen pickup was observed. However, due to the long processing time, the colony size became much larger, which might influence the mechanical properties unfavourably. The importance of a fine microstructure for good e.g. fatigue behaviour of MIM processed components made from Ti–6Al–4V powder is discussed in [6].

Table 7
Mean pore size, standard deviation and P_{90}, for MIM samples sintered at 1623 K, with different sintering time.

Sintering time (h)	Mean pore size (μm)	Standard deviation (μm)	P_{90} (μm)
1	15	11	28
2	15	10	27
10	15	11	26

3.4. Tensile fractography

The Ti–6Al–4V alloy specimens' fracture surfaces are shown in Fig. 6(a–d). A clear difference in fracture surface behaviour amongst the different sintering parameters is observed. The specimens sintered at lower temperatures (Fig. 6a) and the specimens with a heating rate dT_{sinter} of 15 K/min (Fig. 6b) exhibit big cavities apart from the existing pores and few dimples on the tensile fracture surface. This behaviour can be an indication of a mixed fracture mechanism (transgranular and intergranular). The sample may have fractured intergranularly in some areas where the connections between the grains were not well established due to an incomplete sintering process, and in other areas, the samples presented a typical ductile fracture surface with fine dimples (white arrows indicate the fine dimples on the tensile fracture surface). The presence of finely dimpled structure on the tensile fracture surface was much more pronounced for samples sintered at 1623 K with a heating rate dT_{sinter} of 5 K/min (Fig. 6c). A possible explanation for such behaviour can be related to the sintering process. As described by German [7], the two main mechanisms of densification and coarsening describe the sintering behaviour of a specific material. For most materials, during the final sintering process (usually at relatively high temperatures), the coarsening effect overcomes the densification effect mainly due to a phenomenon called "breakaway". Breakaway is the isolation of the pores into grain interiors. This occurs due to the fact that beyond certain point the driving force for grain growth exceeds the pore restraining force.

Therefore, at a higher heating rate dT_{sinter}, one can expect that the coarsening mechanism will be activated earlier than at a lower heating rate as discussed above. The results of grain size and densification for the samples sintered with heating rates of 5 and 15 K/min illustrated in Table 4 support to this assumption. In fact, it should be noted that the lower presence of fine dimples on the tensile fracture surface of samples sintered at lower temperatures or with higher heating rate is an indication of a sintering process that is not optimal.

Table 6
Variation of sintering time. Sintering temperature 1623 K, binder content 10 wt.%, heating rate dT_{sinter} of 10 K/min.

Sintering time (h)	Tensile properties			Microstructural features	
	Yield stress (MPa)	UTS (MPa)	Elongation (MPa)	Average colony size (μm)	Densification (%)
1	699 ± 5	801 ± 5	13.9 ± 0.1	94 ± 3	94.6
2	720 ± 2	824 ± 4	14.3 ± 0.7	93 ± 2	95.7
10	753 ± 1	853 ± 1	13.0 ± 0.2	157 ± 8	98.0

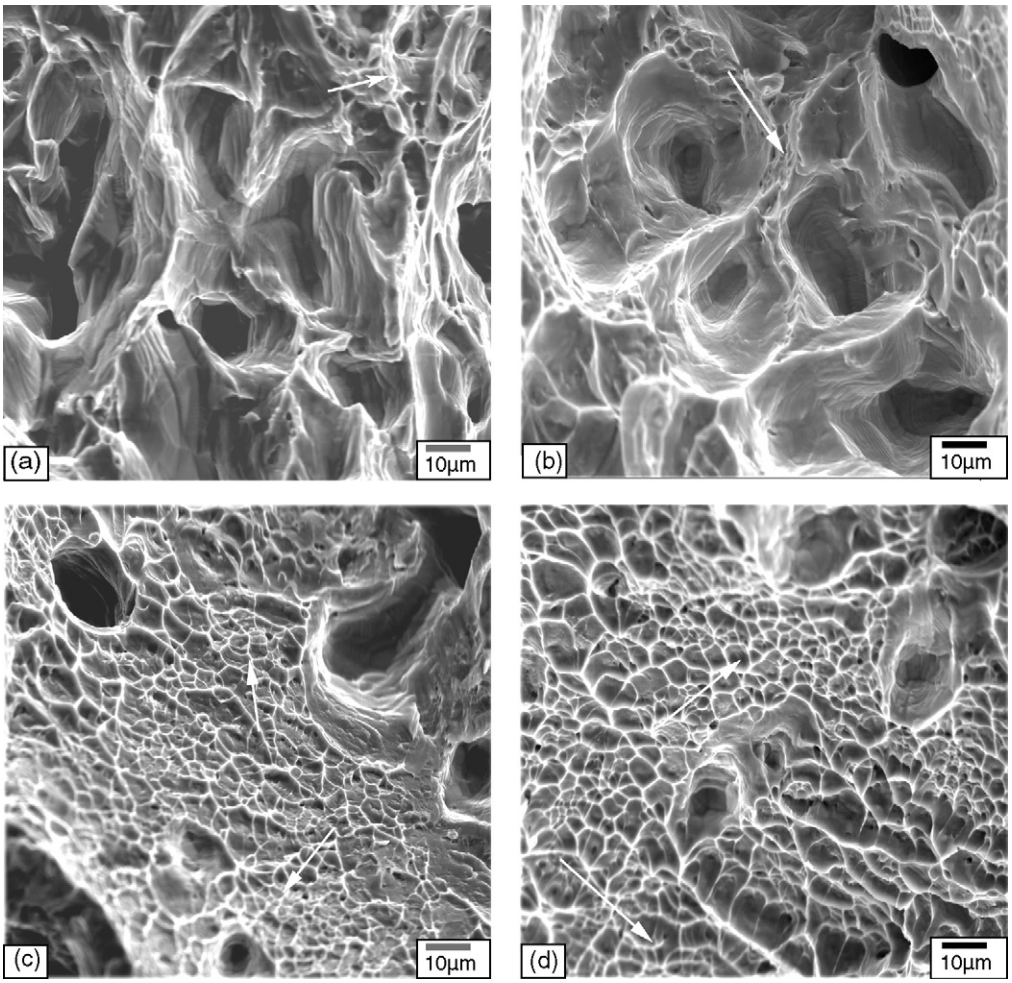

Fig. 6. SEM in BSE mode micrographs of the fracture surfaces of samples sintered (a) at 1523 K (b) at 1623 K with heating rate dT_{sinter} of 15 K/min, (c) at 1623 K with heating rate dT_{sinter} of 5 K/min and (d) at 1623 K sintered for 10 h (10% binder content).

Fig. 6d shows the fracture surface of a sample with 35 vol.% binder content sintered for 10 h. It is entirely covered by fine dimples and corresponds very well with the fracture surface sample with 31 vol.% binder that was sintered for 2 h, shown in Fig. 6c. In summary, the amount and structure of dimples appear to correspond with the strength of the samples, as indicated in Tables 4 and 6. However, it is important to note that it was not possible to relate the amount of dimples to the final plastic elongation, since samples sintered at 1523 K exhibited almost no dimples, but still showed a plastic elongation in the range of samples sintered at 1623 K which had a high amount of fine dimples. As of yet, it is not possible to totally understand, on micromechanical level, the influence of pores and maximum sintering temperature on the ductility, especially when the samples exhibit a relatively low fraction of remaining pores.

3.5. Variation of cooling rate

The variation of the cooling rate after sintering is presented in Table 8. A significant, but unsystematic influence on the tensile properties of the sintered part was observed. While the samples cooled at a rate of 20 K/min reveal approximately the same tensile strength as but a higher ductility than the reference samples cooled at a rate of 10 K/min, a small but significant improvement of the tensile strength was observed by applying a slower cooling rate of 5 K/min. The strength is increased by about 10 MPa and the plastic elongation by about 2%. It can be assumed that the improved tensile property is mainly due to the lower porosity, which was connected to the longer over-all time the sample is exposed to high temperature.

On the other hand, the highest strength was accomplished by using a cooling rate of 66 K/min, which corresponds to a simple switch off of the furnace used. The rate was calculated from the time of uncontrolled cooling from 1623 K to 1273 K. Although the densification was relatively low, the observed improvement in strength was expected due to the decrease in α lamellae width as given in Table 8. It has been reported by Filip et al. [8] and Lütjering [9] that the mechanical properties strongly depend on the applied cooling rate since microstructural features such as α lamellae colony width, α colony size, and β grain size are affected. The observed microstructure showed that the width of α lamellae decreased by almost half compared to that of the standard process. This is visible in Fig. 7 showing the SEM micrographs of the two different cooling rates 10 K/min and 66 K/min.

3.6. Variation of heating rate to debinding temperature dT_{debind}

The heating rate dT_{debind} denotes the temperature change per minute from room temperature to the debinding isotherm, in this study fixed at 723 K. The thermal debinding process can influence the mechanical properties on two ways. Firstly, during decomposition of the polymer, carbon can diffuse into the alloy powder as an interstitial element, and secondly, accelerated debinding can destroy the structure of the part by pressure build-up. Therefore,

Table 8
Variation of cooling rate. Sintering temperature 1623 K, heating rate dT_{sinter} 5 K/min.

Cooling rate (K/min)	Tensile properties			Microstructural features		
	Yield stress (MPa)	UTS (MPa)	Elongation (%)	Average colony size (μm)	Densification (%)	α Lamellae width (μm)
5	739 ± 3	842 ± 2	15.5 ± 1	113 ± 5	97.3	14
10	728 ± 5	832 ± 2	13.4 ± 1	102 ± 3	97.1	14
20	731 ± 2	835 ± 1	14.4 ± 1	92 ± 2	96.8	10
66	757 ± 4	861 ± 4	14.3 ± 0.4	95 ± 3	96.8	7

Table 9
Variation of heating rate dT_{debind}. Sintering temperature 1623 K, heating rate dT_{sinter} 5 K/min.

Heating rate dT_{debind} (K/min)	Tensile properties			Microstructural features		
	Yield stress (MPa)	UTS (MPa)	Elongation (%)	Average colony size (μm)	Densification (%)	Carbon content (μg/g)
2	728 ± 5	832 ± 2	13.4 ± 0.5	91 ± 2	97.1	400 ± 34
5	734 ± 3	835 ± 2	14.0 ± 0.4	92 ± 3	97.1	395 ± 14
10	728 ± 3	828 ± 4	13.5 ± 1	92 ± 2	97.1	403 ± 47

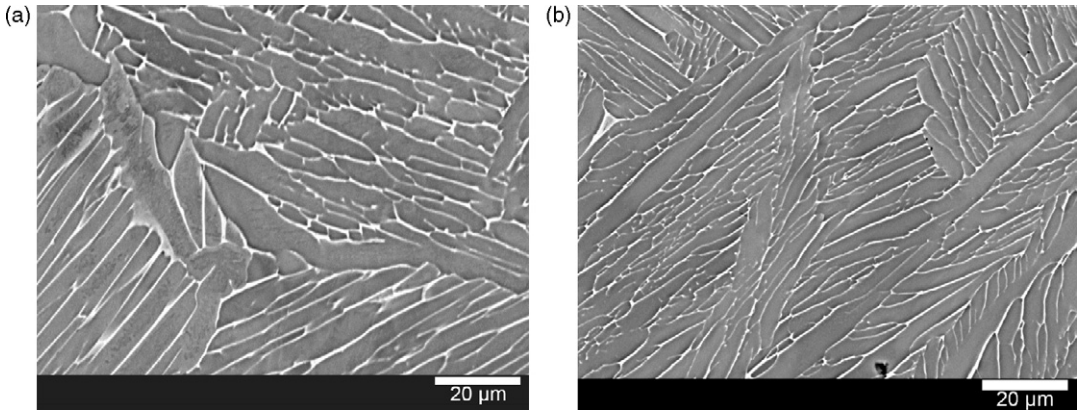

Fig. 7. Comparison of α lamellae width in two samples cooled with rate of (a) 10 K/min and (b) 66 K/min. The white features represents the β-phase, the dark ones the α-phase.

a possible effect of the heating rate dT_{debind} on the mechanical properties was investigated.

Table 9 shows the test results of the samples debound at different heating rates and sintered at 1623 K. The table indicates similar tensile properties and identical densification of all parts.

As illustrated in Table 9, there was no significant change in the carbon content of the compacts. The observed slight difference in the average value of the carbon content compared to the average value quoted for all the samples investigated could be attributed to the usual scattering of about 50 μg/g due to the furnace atmosphere. This indicates that the binder was completely removed at all investigated heating rates. Furthermore, even the samples debound with a higher heating rate dT_{debind} did not show any surface defects. This result agrees with previous investigation of Yimin et al. [10], who reported that increasing the heating rate did not promote defects in compacts with thicknesses smaller than 10 mm. One has to keep in mind, though, that the optimal heating rate depends on the geometry of the particular component. Nevertheless, it can be concluded from this study that there is a rather wide scope within which this parameter can be varied without influencing the properties of the sintered part.

4. Summary and conclusion

The essential process parameters for thermal debinding and sintering within the MIM processing of Ti–6Al–4V were varied in order to investigate their specific influence on the mechanical properties of the sintered parts. The study was aimed at both optimising the mechanical properties and obtaining better knowledge that can be directed towards process controlling during production.

A clear dependence of the tensile strength on the sintering temperature and time due to differences in densification was observed, while the interstitial content remained constant. On the other hand, the microstructure became coarser because of sintering at higher temperatures or longer times, which might deteriorate e.g. fatigue behaviour.

Within the range of 2.0–5.4% residual porosity observed in this study, no clear influence of the density, pore size and pore shape on the plastic elongation was detected.

The heating rate to debinding temperature dT_{debind} can be varied within a rather large range without affecting the properties of the sintered parts. This indicates that this parameter is not critical and should be adjusted, aiming for short processing times.

Contrary to dT_{debind}, the subsequent heating rate dT_{sinter} up to the sintering temperature appears to be critical and influences final density and grain size. A 10 K/min heating rate should not be exceeded for the powder used in this study.

Fast cooling is beneficial with respect to mechanical properties due to the establishment of fine α lamellae. Simultaneously, a favourable shorter processing time can be achieved.

Taking into account all these factors, tensile properties of $\sigma_{0.2}$ = 757 MPa, UTS = 861 MPa and ε = 14.3% were achieved in this

study. These mechanical properties meet the requirements of the ASTM B 348-02 for grade 23. Furthermore, it is important to note that Zhang et al. [4] obtained an even higher tensile strength, but this was achieved not without detriment to plastic elongation. However, in this investigation, the increase of tensile strength was accompanied by retained excellent ductility. Such a result was possible due to the fact that the pick up of interstitial elements during the sintering process was relatively low and constant.

Acknowledgement

This project has been funded by European Commission–Education.

References

[1] F.H. Froes, J. Lombardi, L. Lavoie, J. Fravel, M. Godfrey, In: F.H. (Sam) Froes, E.Y. Chen, R.R. Boyer, E.M. Taleff, L. Lu, D.L. Zhang, C.M. Ward-Close, D. Eliezer (Eds.), TMS, Seattle, 2002, p. 4.
[2] B. Oger, T. Ebel, W. Limberg, EUROPM 2006, vol. 2, EPMA, 2006, pp. 191–196.
[3] Y. Itoh, T. Harikou, K. Sato, H. Miura, PM World Conf. 4 (2004).
[4] R. Zhang, J. Kruszewski, J. Lo, Powder Inject. Mould. Int. 2 (2008) 74–78.
[5] E. Aust, W. Limberg, R. Gerling, B. Oger, T. Ebel, Adv. Eng. Mater. 8 (2006) 365–370.
[6] O.M. Ferri, T. Ebel, R. Bormann, Mater. Sci. Eng. A 504 (2009) 107–113.
[7] R.M. German, Powder Metallurgy Science, MPIF, Princeton, 1984.
[8] R. Filip, W.Z.K. Kubiak, J. Sieniawski, J. Mater. Process. Technol. 2003 (2003) 84–89.
[9] G. Lütjering, Mater. Sci. Eng. A 243 (1998) 32–45.
[10] L. Yimin, F. Jiang, L. Zhao, B. Huang, Mater. Sci. Eng. A 362 (2003) 292–299.